RADIO SCIENCE, VOL. 44, RS2005, doi:10.1029/2008RS003876, 2009

Analysis and improvements of cloud models for propagation studies

V. Mattioli,[1] P. Basili,[1] S. Bonafoni,[1] P. Ciotti,[2] and E. R. Westwater[3]

Received 16 April 2008; revised 6 November 2008; accepted 12 January 2009; published 20 March 2009.

[1] Two cloud models currently in use in propagation and remote sensing simulations in the presence of nonprecipitating clouds were analyzed. A new cloud model is also proposed: a modification of a humidity threshold to better identify clouds is suggested, as is a new cloud density function for computing cloud liquid and ice content within a cloud. The performances of the threshold functions were examined at the Atmospheric Radiation Measurement (ARM) Program's Southern Great Plaints (SGP) site in Oklahoma, USA, by using radiosonde and ceilometer data. The new threshold showed an improvement in the cloud detection (15%) and a reduction of false cloud identification in clear-sky conditions (26%). Next, the cloud density models were evaluated in the brightness temperature (Tb) domain, by comparing simulated Tb values in cloudy conditions with those measured by dual-channel microwave radiometers at several ARM sites. The new model provided good results in comparison with the radiometer measurements, with overall root mean square (RMS) differences of 3.10 K, reducing the RMS by about 16% with respect to the best of the other models. Improvements can be noticed in particular at SGP (20%), and in the tropics (37%).

Citation: Mattioli, V., P. Basili, S. Bonafoni, P. Ciotti, and E. R. Westwater (2009), Analysis and improvements of cloud models for propagation studies, *Radio Sci.*, *44*, RS2005, doi:10.1029/2008RS003876.

1. Introduction

[2] The assessment of the impairments on microwave signal propagation due to atmospheric gases and clouds plays a critical role in both radio propagation problems [*Salonen and Uppala*, 1991; *ITU-R*, 1999, 2007; *Garcia et al.*, 2008] and remote sensing studies [*Liebe*, 1989; *Westwater*, 1993; *Hanssen*, 1998]. As satellite services are increasingly offered at higher frequencies, a complete understanding of the influence of the atmosphere on microwave propagation is needed, especially for Ka-band channels and above [*Watson and Hu*, 1994; *Alouini et al.*, 1997; *Dissanayake et al.*, 2001; *Lemorton et al.*, 2001; *Castanet et al.*, 2001; *Martellucci et al.*, 2002a; *Green*, 2004]. Major factors impairing Ka-band satellite communication include rain attenuation, gaseous absorption, cloud attenuation, melting layer attenuation, rain and ice depolarization and tropospheric scintillation. Precipitation is the main impairment factor for millimeter wave signals propagating through the atmosphere. However, for systems involving Ka-band and V-band low-margin small aperture terminals, rain effects may only form a relatively small part of the total propagation link margin. Conversely, the frequent presence of clouds may cause significant fades in these bands for a large portion of the time. Many efforts have been devoted to investigating cloud attenuation [*Slobin*, 1982; *Salonen and Uppala*, 1991; *Al-Ansari et al.*, 2003; *Sarkar et al.*, 2005; *Mandeep and Hassan*, 2008] and simple models that make use of a few effective parameters have been developed [*Altshuler and Marr*, 1989; *Dintelmann and Ortgies*, 1989; *Dissanyake et al.*, 1997; *ITU-R*, 1999; *Wrench et al.*, 1999]. Moreover, synthetic data sets of propagation parameters are often generated for this purpose from radiosonde observations and/or atmospheric profiles derived from numerical weather prediction model (NWP) analyses [*Martellucci et al.*, 2002a; *Pierdicca et al.*, 2006; *Luini et al.*, 2007].

[3] The simulation of electromagnetic parameters such as atmospheric attenuation and brightness temperatures (Tb values) can be generated using accurate physical models implemented in a plane parallel radiative transfer scheme [*Schroeder and Westwater*, 1991]. The extinction

[1]Dipartimento di Ingegneria Elettronica e dell'Informazione, Università di Perugia, Perugia, Italy.

[2]Dipartimento di Ingegneria Elettrica e dell'Informazione, Università di L'Aquila, Poggio di Roio, L'Aquila, Italy.

[3]Center for Environmental Technology, Department of Electrical and Computer Engineering, University of Colorado, Boulder, Colorado, USA.

0048-6604/09/2008RS003876$11.00

Table 1. Site Name, Location, Instruments, and Temporal Coverage of the ARM Data Used in This Work

Site	Location	Latitude (°N)/Longitude (°E)	Time Period	Instruments
SGP	Lamont, Oklahoma	36.61/−97.49	2002–2006	RAOBs, VCEIL, MWR
PYE	Point Reyes, California	38.09/−122.96	Mar.–Nov. 2005	RAOBs, VCEIL, MWR
NSA	Barrow, Alaska	71.32/−156.62	2003–2006	RAOBs, VCEIL, MWR
TWP	Manus, Papua New Guinea	2.06/147.43	2003–2006	RAOBs, VCEIL, MWR
FKB	Heselbach, Black Forest, Germany	48.54/8.4	Apr.–Dec. 2007	RAOBs, VCEIL, MWR

by small cloud droplets [*Westwater*, 1972; *Liebe et al.*, 1991; P. W. Rosenkranz, private communication, 2003] is computed in general from cloud water (both liquid and ice) density profiles by adopting the Rayleigh approximation of the Mie scattering theory, under which absorption is considered independent of cloud particle size distribution, and scattering is considered negligible relative to absorption. The validity of this approach, which is the one considered in this paper, is therefore restricted to nonprecipitating clouds with particle radii smaller than 100 μm for frequencies less than 100 GHz [*Ulaby et al.*, 1981].

[4] Since radiosondes generally do not measure cloud water density, models are necessary to estimate cloud liquid and ice density profiles required for the simulations of the atmospheric parameters in cloudy conditions. In this work, we analyze two cloud models that are currently in use in propagation and remote sensing simulations in the presence of nonprecipitating clouds: the model proposed by *Decker et al.* [1978], (hereafter the Decker model) and the model proposed by *Salonen and Uppala* [1991], modified for the ice contribution by *Martellucci et al.* [2002b] (hereafter the Salonen model). In this analysis, we examine first the performances of the threshold functions used for detecting the presence of clouds by using ceilometer data for comparison of cloud bases. In addition, the cloud density models are evaluated in the brightness temperature (Tb) domain, by comparing the Tb values simulated in cloudy conditions with those measured by dual-channel microwave radiometers at 23.8 and 31.4 GHz. Finally, a new cloud model is proposed: we modified the Salonen humidity threshold to improve the capability to identify clouds, and develop a new cloud water density function for computing cloud liquid and ice content within a cloud. The performances of the thresholds were assessed at the Atmospheric Radiation Measurement (ARM) Program's Southern Great Plaints (SGP) site in Oklahoma, USA, by using data from radiosondes and a ceilometer. To tune and evaluate the parameters included in the proposed cloud density model over a wide range of atmospheric conditions (tropics to Arctic), as well as to test the general applicability of the three cloud models (Decker, Salonen, and new model) we used data collected at several ARM sites. More specifically, data were collected at the three primary and fixed locations (SGP, Tropical Western Pacific (TWP) at Manus, Papua New Guinea, North Slope of Alaska (NSA) in Point Barrow, Alaska, USA) and at the ARM Mobile Facilities in Point Reyes (PYE), California, USA, and in the Black Forest (FKB), Germany, for the period of their deployment. The site name, location, instruments, and temporal coverage of the data used are given in Table 1.

[5] As an intermediate step in our analysis, after the tuning of the Salonen threshold function, we also tuned and evaluated the parameters of the Salonen water density model, to investigate the effectiveness of the Salonen approach, and results suggested us to examine a different function.

2. Cloud Model Description

2.1. Decker Model

[6] The Decker model identifies clouds from atmospheric profiles by comparing the relative humidity (RH) profile with a threshold given by a constant RH value, which in this work was set both to 90% and to 95%. The suggested value in the work of *Decker et al.* [1978] was 95%, while 90% or slightly lesser was widely used in the past [*Han and Westwater*, 1995; *Wang et al.*, 2000; *Minnis et al.*, 2005]. Cloud layers are identified in the profile when the atmospheric RH exceeds the RH threshold. This model assumes that the total cloud water content TWC (g m^{-3}), considered as the sum of cloud liquid water and ice contents, LWC and IWC respectively, within a given cloud is constant with height, with values depending on the cloud thickness ΔH (km) as given in equation (1).

$$\begin{cases} TWC = 1.6 \cdot \Delta H \\ \mathrm{Min}(TWC) = 0.2 \\ \mathrm{Max}(TWC) = 0.8 \end{cases} \quad g \cdot m^{-3} \tag{1}$$

For each cloud profile, three density values are given, which are obtained by multiplying the TWC in equation (1) by a parameter γ that can assume the values of 1, 0.5 and 0.25, corresponding therefore to three density models [*Decker et al.*, 1978]. Among them, we have chosen the one ranging from 0.05 to 0.2 g m^{-3} (i.e., γ equal to 0.25), to account for the overestimation of brightness temperatures (Tb values) and of integrated values of LWC (liquid water path (LWP)), given by the

other two models. Further discussion and evaluation of these models is presented in section 6.

[7] Then, for each identified cloud layer, the fraction of cloud water content treated as liquid water or ice is computed, depending on the air temperature T (°C), according to equation (2):

$$\begin{cases} IWC = 0 & LWC = TWC & T > 0 \\ IWC = TWC \cdot ({}^{T}/_{30})^4 & LWC = TWC - IWC & -30 < T \le 0 \\ LWC = 0 & IWC = TWC & T \le -30 \end{cases} \tag{2}$$

2.2. Salonen Model

[8] The Salonen model identifies clouds when the relative humidity exceeds the critical humidity function RHc in equation (3):

$$RHc = 1 - \alpha\sigma(1-\sigma)[1 + \beta(\sigma - 0.5)] \tag{3}$$

where σ = P(i)/P(0), and P(i) and P(0) are the pressures (hPa) at the considered atmospheric ith level and at the ground, respectively. The two empirical parameters in equation (3) are α = 1.0 and $\beta = \sqrt{3}$.

[9] The total cloud water content within each cloud layer is a function of the height above the cloud base and of the temperature in the layer as given in equation (4):

$$TWC(h,T) = \begin{cases} w_0 \left(\dfrac{h - h_b}{h_r}\right)^a \cdot (1 + cT) & T \ge 0°C \\ w_0 \left(\dfrac{h - h_b}{h_r}\right)^a \cdot (\exp(cT)) & T < 0°C \end{cases} \tag{4}$$

where $w_0 = 0.17$ g m^{-3}, h and h_b are the heights (km) above the surface and of the cloud base, $h_r = 1.5$ km, a = 1, and c = 0.04°C^{-1}. LWC and IWC are given by equation (5):

$$\begin{aligned} LWC &= TWC(h,T) \cdot f_W(T) \\ IWC &= TWC(h,T) \cdot [1 - f_W(T)] \end{aligned} \tag{5}$$

where the fraction of cloud liquid f_W is given by equation (6):

$$f_w(T) = \begin{cases} 1 & T \ge 0°C \\ 1 + T/20 & -20 \le T < 0°C \\ 0 & T < -20°C \end{cases} \tag{6}$$

3. Humidity Threshold Analysis and Optimization

3.1. Decker and Salonen Threshold Performances

[10] In this section, we evaluate the capability of the Decker and Salonen models to predict the presence of clouds. Different approaches for cloud detection by using radiosonde profiles (RAOBs) have also been used, as summarized in the work of *Naud et al.* [2003]. *Chernykh and Eskridge* [1996] predicted cloud layers by computing the second derivative of the temperature and relative humidity vertical profiles. Recently, this algorithm was improved by *Bouchard* [2005] supplemented by retrievals from a 12-channel radiometer profiler, and used to compute statistics of LWP and cloud boundaries over Ottawa [*Bouchard and Rogers*, 2006].

[11] Here, cloud base heights determined from the radiosoundings by using the Decker and the Salonen humidity thresholds were compared with the cloud bases measured by a ceilometer. The analysis was performed by using data collected at the ARM SGP site during years 2005 and 2006. Radiosondes of the Vaisala RS92 type were regularly launched four times a day (0530, 1130, 1730, 2330 UTC) at the SGP site, and the ceilometer was a Vaisala CT25K model (VCEIL) that measured cloud base heights up to a nominal altitude of 7.5 km on a 15-s temporal scale.

[12] Our comparison was performed as follows: for every radiosounding, the relative humidity profile was compared with the thresholds, and cloud bases when present were recorded; otherwise, a cloud free case was recorded. Then, 1-h measurements from the VCEIL starting from the radiosonde launch time were also recorded, and the average cloud base and the standard deviation (std) were computed in this interval. VCEIL measurements were classified as clear sky when no cloud bases were found in the selected temporal interval and as cloudy when cloud bases were identified for more than 50% of the period. We selected for suitable comparison only cloudy cases for which the cloud base std from the ceilometer was less than 200 m. This last condition was adopted in order to examine cloudy situations with a quite uniform cloud base, and to compute an average cloud base that was representative of the VCEIL measurements. In addition, concerning the radiosonde spatial displacement from the launch site due to the presence of wind, we have adopted the criterion of accepting radiosoundings for which the horizontal displacement that was reached by the radiosonde at an altitude of 6 km was less than 25 km. This distance was computed by using the wind information (wind direction and speed) that is routinely available in the radiosonde data at SGP, and computed by using the recorded elevation and azimuth information from the radiosonde tracking system. Applying this constraint, about 1/5 of our data set was discarded. The results of our comparisons are summarized in Table 2. A number of 1406 RAOBs were analyzed, chosen during nonrainy conditions for the 2-year period, and satisfying the displacement criterion.

[13] In Table 2, the first column reports the percentage of correct detection of clear-sky cases from the threshold, with respect to the VCEIL measurement. Conversely, the

Table 2. Cloud Base Height Detection[a]

	Clear Sky		Cloudy Conditions		
	Correct Detection	False Alarm	Correct Detection (±200 m)	Incorrect Detection (>200 m)	Missed Detection
Decker 0.9	88.1%	11.9%	21%	76.5%	2.5%
Decker 0.95	94.9%	5.1%	52.5%	40.9%	6.5%
Salonen	60%	40%	42.8%	57.8%	0%

[a]Decker and Salonen performances (1406 cases, 1130 clear sky, 276 cloudy, RAOBs, 2005–2006).

second column reports the percentage of false cloud occurrence, which took place when the RH threshold from a model identified a cloud while the VCEIL did not. Both percentages were computed over the total clear-sky cases (1130). The third column reports the percentage of correct cloud base detection by the threshold, with respect to the average cloud base measured by the VCEIL. We have considered that a cloud base was correctly identified by the threshold when the two cloud bases agreed within 200 m. The fourth column gives the percentage of incorrect detection, which occurred when the cloud bases differed for more than 200 m. Finally, the last column gives the missed detection percentage, which occurred when the model threshold evaluated clear sky while the VCEIL identified a cloud. These last three column percentages were computed with respect to the total cloudy cases (276), as identified by the VCEIL. In our analysis, we have also considered an averaging time of the ceilometer measurements of 20 min instead of 1 h, but the results as given in Table 2 did not change appreciably.

[14] From Table 2, we note that the Salonen threshold provided poorer results with respect to the Decker constant values (both 0.9 and 0.95) during clear-sky conditions, with 40% of false alarms with respect to 12% and 5%, respectively. This was due to a misclassification of clear but moist atmospheric layers as clouds by the Salonen threshold, in particular in the middle troposphere. Conversely, in cloudy conditions the Decker 0.9 constant threshold produced the poorest results, with a correct detection percentage of 21% against 52% of the Decker 0.95, and 43% of the Salonen threshold. These results are explained considering that a constant threshold as in the Decker model tends to misinterpret a clear but very moist layer as a cloud in the boundary layer, and this is more evident as lower is the constant value. Also, it might misinterpret a cloudy layer drier than 95% as a clear layer in the middle troposphere (6.5%).

[15] To better understand the results of Table 2, we show in Figure 1 the scatterplots of the cloud bases identified from the RAOBs by the three thresholds versus the cloud bases measured by the VCEIL. The Salonen threshold function seems to identify low clouds quite correctly with respect to the Decker one, but provides poorer results mainly in the middle troposphere, where the cloud base detected from the VCEIL is always higher than that one from the Salonen threshold (starting from about 1.5 km above the surface). The Salonen threshold generally gives too low RH values that can be as low as 71% in the middle troposphere for cloud identification, resulting in the high percentage (58%) of incorrect detection in Table 2, with the cloud base from RAOBs being always lower than that one from the VCEIL, and in the high percentage of false cloud alarm in clear-sky conditions (40%).

3.2. Salonen Humidity Threshold Optimization

[16] In this section, we modified the Salonen humidity threshold function to improve its cloud detection capabilities both in the boundary layer and in the middle troposphere. The optimization of the RHc threshold as in equation (3) was performed by tuning the function to the ceilometer data [*Basili et al.*, 2006]. We used a large data set of RAOBs and ceilometer measurements collected during years 2002, 2003, and 2004 at the ARM SGP site. Data from years 2005 and 2006 were used as an independent data set for the validation of the threshold, and for adequate comparison with the results given in section 3.1.

[17] Although radiosondes provide accurate temperature and humidity profiles with respect to remote sensors, differences in temperature and humidity profiles from various sensor types are known [*Schmidlin et al.*, 1986; *Wang et al.*, 2003; *Mattioli et al.*, 2007]. ARM collected radiosonde data since 1992, nevertheless, a general problem with Vaisala RS-80H radiosondes (the type used by ARM from May 1992 through spring 2002) was that they exhibited a dry bias; that is, the relative humidity values reported were too low [*Wang et al.*, 2002; *Turner et al.*, 2003]. The amount of the error varied with several factors including the ambient temperature and relative humidity and the age of the radiosonde but could be as large as 10% RH. Therefore, radiosonde type and processing can affect the choice of threshold values used to identify the cloud presence. With the intent of selecting a suitable data set for the optimization, in our analysis we have considered only Vaisala of the RS90/92 type. Nevertheless, *Miloshevich et al.* [2006] and *Vömel et al.* [2007] found that a diurnal 5% dry bias is still present.

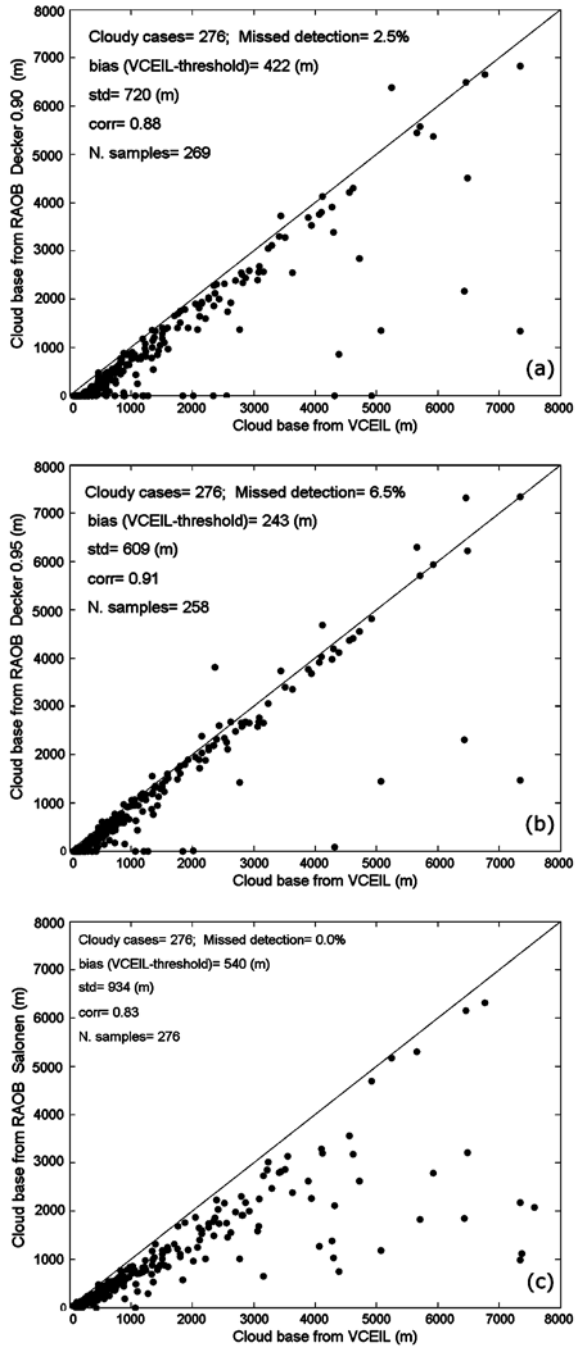

Figure 1. Comparison between cloud bases from Decker and Salonen thresholds and from VCEIL when both see a cloud (years 2005–2006). (a) Decker 0.90 constant value; (b) Decker 0.95 constant value; (c) Salonen threshold.

[18] The following criteria were used to derive the optimization of RHc: relative humidity and normalized σ pressure values were recorded from radiosoundings together with the corresponding cloud base height measured by VCEIL. The correspondence (more conservative than the one used in section 3.1) was verified when the difference between the height reached by the radiosounding and the VCEIL cloud base height was within 100 m and the time in which the radiosonde reached that height and the time of VCEIL measurements was within 2 min. Concerning the radiosonde horizontal displacement from the launch site due to the presence of wind, we discarded the radiosondes with a displacement greater than 5 km when a cloud was detected. Afterward, the final data set included 2098 RH and σ values ascribed to vertical atmospheric layers with a thickness of 100 m, uniformly distributed from near the surface up to an altitude of 7.5 km.

[19] To optimize the RHc function the profile of the mean values of the selected RH data set minus one standard deviation was computed as a function of σ values. Then, a nonlinear least squares data fitting of this vertical profile was performed in order to estimate the new fitted coefficients of the RHc function, providing $\alpha = 0.59$ and $\beta = 1.37$. Hereafter, this threshold function will be referred to as Salonen08. The various threshold functions are shown in Figure 2, together with a sample RH profile. The comparison of Salonen08 threshold with the VCEIL is summarized in Table 3 for years 2005–2006, analogous to the analysis we performed in section 3.1.

[20] Analyzing the performances of the new threshold, we can note an improvement in the cloud detection of a 15% with respect to the Salonen threshold due to the higher RHc values in the middle troposphere, and a reduction of false cloud alarm in clear-sky conditions of 26%. Also, with respect to the constant thresholds of the

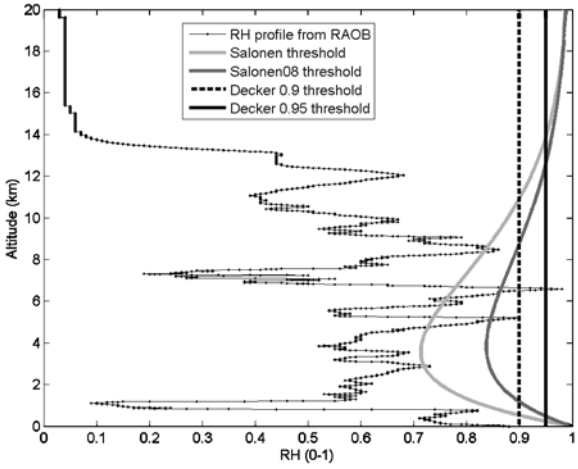

Figure 2. Threshold critical functions applied to a RH profile taken on 1 June 2003.

Table 3. Cloud Base Height Detection[a]

	Clear Sky		Cloudy Conditions		
	Correct Detection	False Alarm	Correct Detection (±200 m)	Incorrect Detection (>200 m)	Missed Detection
Salonen08	86.2%	13.8%	58%	41.3%	0.7%

[a]Salonen08 performances (1406 cases, RAOBs, 2005–2006).

Decker model, there is an error reduction in cloud detection especially in the boundary layer due to the greater critical humidity (as for the Salonen threshold).

4. Comparison With MWRs at ARM Sites

[21] To evaluate the cloud models described in section 2 (equations (1)–(4)), those models were included in a radiative transfer algorithm to simulate brightness temperatures in cloudy conditions and in the absence of scattering [*Schroeder and Westwater*, 1991]. The model proposed by *Rosenkranz* [1998, 1999, also private communication, 2003] for gaseous absorption has been used in applying the radiative transfer scheme. Liquid water and ice absorption were computed as given in the work of *Westwater* [1972], with liquid absorption modified by P. W. Rosenkranz (private communication, 2003). For the Salonen cloud model, both the original and the modified critical humidity threshold functions were applied.

[22] To evaluate the applicability of the various models to different geographic areas, being cloud water content dependent from diverse climatologic and temperature regimes [*Lemus et al.*, 1997; *Gultepe et al.*, 2002], our analysis was performed by using data collected at several ARM sites. The data set used in this comparison is part of our available data set given in Table 1. Data were from the ARM SGP during the years 2003 and 2004, the ARM PYE for about three months of the six-month experiment in 2005 (odd indexed of the whole data set, split into two halves), the ARM NSA during 2005–2006, the ARM TWP during the 2003–2004 period, and finally the ARM FKB Mobile Facility during April–December 2007 (odd data set), with different years used from the ARM primary sites to have interannual variability in our data set. The same data set was also used for tuning the parameters in the Salonen model, and for the development of a new model, as described in section 5. A similar data set, collected at the ARM sites for different periods, was used as an independent test of the tuning procedure and final analysis in section 6.

[23] Radiosondes of the Vaisala RS90 and RS92 type were launched four times per day during the deployment periods at PYE and FKB, respectively; Vaisala RS90/92 were launched once a day until April 2006 at NSA, and twice a day since then; Vaisala RS90/92 were launched two times per day at the TWP Central Facility. Simulated Tb values from the radiosoundings were compared with those measured by dual-channel microwave radiometers (MWRs). The comparison was performed for cloudy cases that were identified by using ceilometer data, according to the procedure described in section 3.1, by applying constraints on the maximum radiosonde horizontal displacement (25 km) and on the uniformity of the ceilometers cloud base during a 1-h period. This quality control was applied to prevent broken cloud situations, where it was difficult to verify that the same cloud was observed by the drifting radiosondes and the ground-based radiometer. The ground-based MWRs were the operational water vapor radiometers at 23.8 and 31.4 GHz [*Liljegren*, 2000] of the WVR-1100 series manufactured by the Radiometrics Corporation. The accuracy of these radiometers is about 0.4 K RMS [*Mattioli et al.*, 2005]. Each MWR had a wet window sensor mounted on the top of the radiometer that turns a heater on during condensing or precipitating conditions.

[24] In Figure 3 we show the scatterplots of Tb values from the MWRs versus Tb values computed from the RAOBs for the 31.4-GHz channel, which is mainly sensitive to liquid water emission. Comparisons are shown respectively for the Decker 0.9 and 0.95 models (Figures 3a and 3b), the Salonen model (Figure 3c), and Salonen model modified with the Salonen08 threshold for cloud detection (Figure 3d). MWR Tb values were averaged within the time interval (±5 min) in which the cloud was detected from RAOBs by the threshold. To avoid rain contamination, radiometer data observed during the time interval between 10 min before and 2 h after rainy events were discarded. Statistical analysis in terms of bias, std, root mean square of the difference (rms), correlation coefficient (corr), and slope and intercept (int) of a linear regression line is also given.

[25] Our analysis shows several features. The Decker model with a RH constant threshold of 0.95 has good agreement with the MWR data, with an almost negligible bias of −0.04 K and a std less than 4 K. Conversely, when the RH threshold of 0.9 is applied, the comparison shows a large positive bias (2.62 K) and std (5.02 K), indicating that too much liquid within a cloud is predicted by the model and this threshold.

[26] The Salonen model yielded a positive bias (0.26 K) and the largest std (7.06 K) with respect to the MWR data,

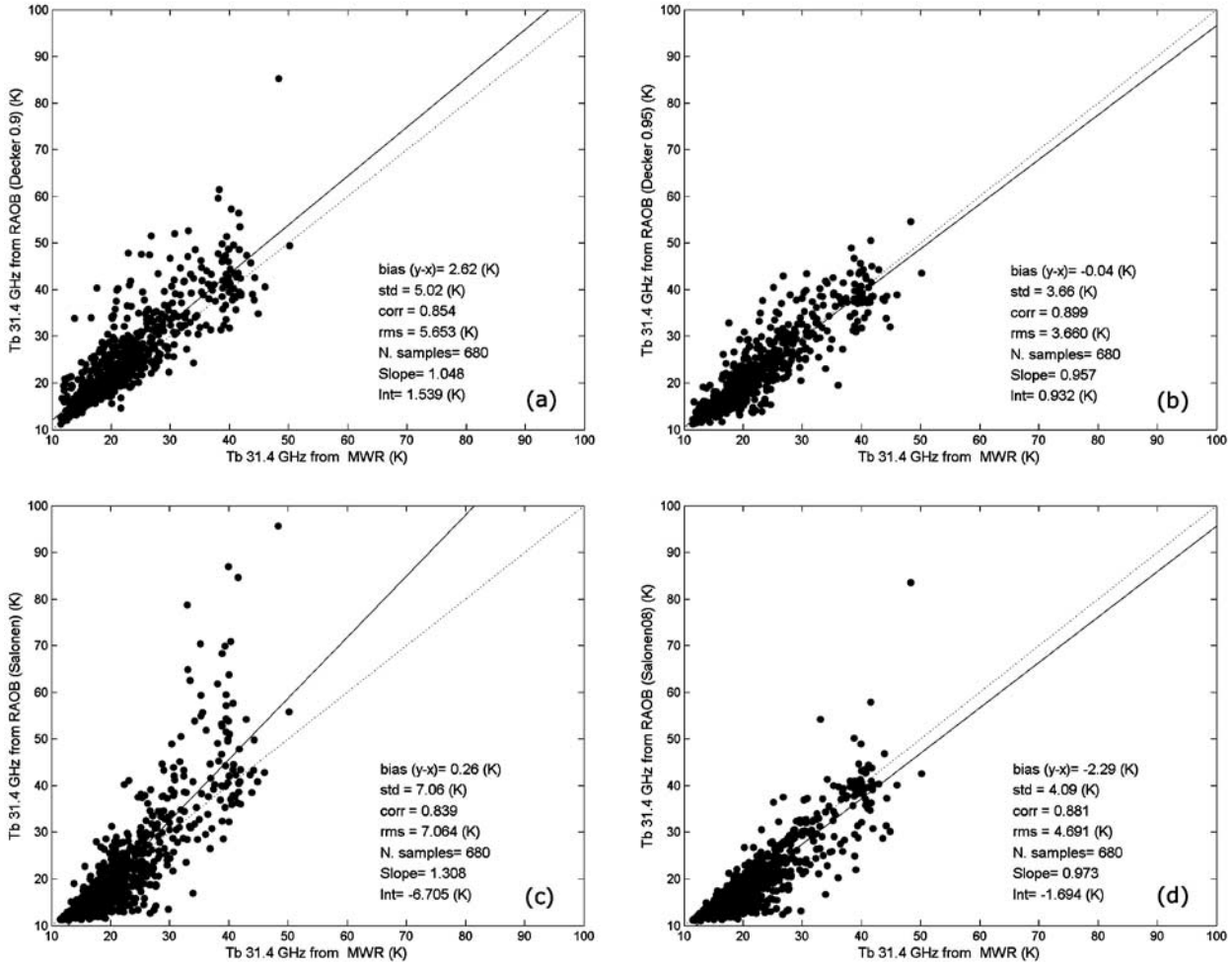

Figure 3. Scatterplots of Tb values at 31.4 GHz measured from the MWRs versus simulated Tb values from radiosondes applying (a) Decker model for cloud water computation (RH threshold constant 0.9); (b) Decker model (RH threshold constant 0.95); (c) Salonen model; (d) Salonen cloud water model and optimized threshold for cloud detection.

mostly due to some high values of simulated Tb values (see Figure 3c). These values arose from cases in which cloud thickness was largely overestimated by the threshold function, which is consistent with results of section 3.1. In fact, introducing the optimized RH threshold function in the Salonen cloud model improved the comparison with the MWR for such cases and reduced the std by about 3 K. Nevertheless, the Salonen08 threshold provided a large negative bias (−2.29 K). Most of the bias is due to cases in the range of Tb values between 20 and 30 K, which are also noticeable in Figure 3c for the original Salonen threshold. All these cases can be associated with low stratiform clouds with small thickness (generally below 500 m).

[27] Such negative bias suggests the following:

[28] 1. Considering the difference in the cloud boundaries obtained by applying the Salonen threshold or the Salonen08, with Salonen08 reducing the cloud thickness, the amount of liquid given by the Salonen model is too low. This suggests that a modification of the Salonen cloud water model is required to tune it to the new threshold. This option is explored in section 5.1.

[29] Similarly, a 5% decrement in the RH threshold constant value in the Decker model (and the consequent increase in cloud thickness and predicted LWP) produced an increment in the Tb values domain of about 2 K in terms of rms.

[30] 2. An adiabatic formulation as in the Salonen model is generally not completely representative of low

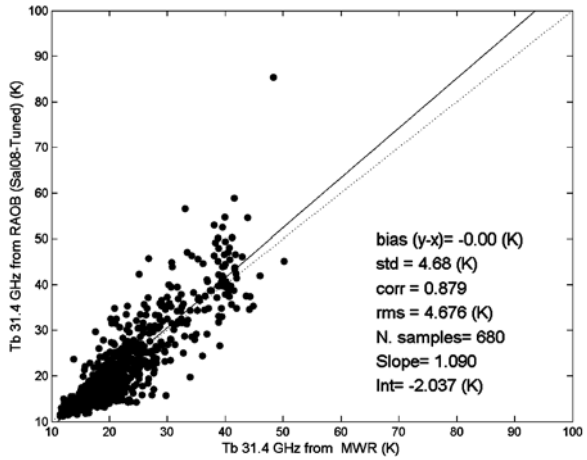

Figure 4. Scatterplots of Tb values at 31.4 GHz measured from the MWR versus simulated Tb values from radiosondes for the Sal08−Tuned model.

stratiform clouds, and therefore a different formulation is required. This option is explored in section 5.2.

[31] As far as the 23.8 GHz channel is concerned (not shown), all models agree quite well with the measurements, although as expected, a similar behavior as for the 31.4 GHz can also be noticed. The RMS between simulated and measured Tb values is 3.7 K, 3.0 K, and 4.3 K for the Decker 0.9, Decker 0.95 and Salonen models, and with a bias respectively of 0.85 K, −0.68 K, and −0.65 K.

5. Cloud Model Refinements

5.1. Tuning of the Salonen Model Parameters

[32] As a consequent step in our analysis, following the conclusions of section 4, we performed a tuning of the Salonen cloud water content model to be adapted to the new threshold [*Mattioli et al.*, 2006]. The tuning was carried out as follows: the four parameters (a, w_0, h_r, c) in the cloud model formulation of equation (4) were varied on a grid with the following ranges: a: from 0.3 to 2.5; w_0: from 0.1 to 0.5 g m^{-3}; h_r: from 0.1 to 3.5 km; c: from 0.011 to 0.091°C^{-1}.

[33] Also, temperatures below which clouds are assumed to be glaciated were evaluated ranging from −20°C (as in the Salonen model) to as low as −35°C, since observations have indicated that liquid drops and ice particles might coexist down to those temperatures [*Korolev et al.*, 2003; *Boudala et al.*, 2004].

[34] Then, for each combination, the same comparison as in Figure 3d was performed and the bias, std, corr, and RMS of the difference between the simulated and measured Tb values were computed. In total, over 6000 different combinations of such parameters were evaluated. The purpose of such analysis was to evaluate quantitatively the sensitivity of the simulated Tb values to the parameters of the model and eventually to tune them to the new humidity threshold, by using well calibrated MWR data. Generally, low std values were associated to strong negative biases. Therefore, to identify the optimum parameter combination, we chose the minimization of the sum of the standard deviation and absolute value of the bias. Relative minima of the above mentioned function were present, ranging from 4.67 K to over 8 K. Minima were found for h_r greater than 0.9 and for w_0 ranging from 0.13 to 0.22. The absolute minimum (4.67 K) was reached for the combination of the following parameters: a = 0.3, w_0 = 0.17 g m^{-3}, h_r = 1 km, c = 0.021°C^{-1}, and cloud glaciation temperature of −35°C.

[35] The comparison of the tuned Salonen model (hereafter referred to as Sal08−Tuned) with the measured Tb values from the ARM MWRs is shown in Figure 4, which shows an improvement of the RMS error of about 34% with respect to the original Salonen model. With respect to the Decker 0.95 model, this last one provided better agreement (of about 1 K) with the MWRs. In the analysis of Figure 4, we noticed that the negative bias associated with low stratiform clouds with small thickness was reduced, but some effect in the Tb range between 20 and 30 K was still present. These results suggested to us to explore a different approach with respect to the adiabatic formulation as in the Salonen model.

5.2. Development of a New Function

[36] In this section, a different density model is proposed. In the Salonen formulation, cloud water content increases

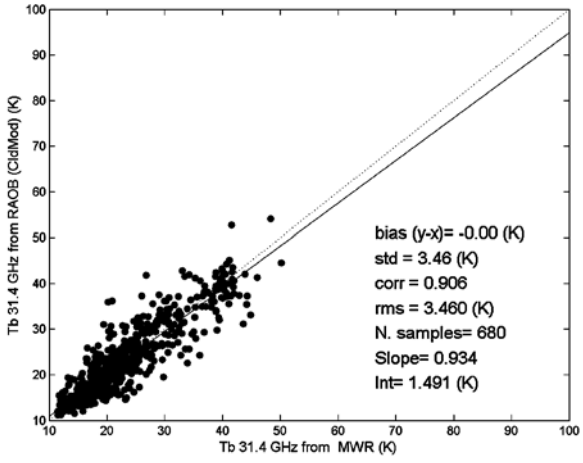

Figure 5. Scatterplot of Tb values at 31.4 GHz measured from the MWR versus simulated Tb values from radiosondes applying the new model (CldMod).

Table 4. Calculations Minus MWR Measurement at the 31.4-GHz Channel[a]

	Decker 0.95	Salonen	Sal08 – Tuned	CldMod
All (Samples 480)				
Bias	0.02	0.75	0.25	0.17
Std	3.72	9.17	4.84	3.10
Corr	0.92	0.85	0.90	0.93
Rms	3.71	9.19	4.84	3.10
Slope	1.05	1.56	1.18	1.00
Int	−1.03	−11.69	−3.79	−0.05
SGP (109)				
Bias	0.78	−0.18	0.65	0.68
Std	3.93	4.34	4.37	3.14
Corr	0.80	0.81	0.77	0.85
Rms	3.99	4.33	4.39	3.19
Slope	0.93	1.08	0.94	0.89
Int	2.32	−2.06	2.05	3.27
PYE (89)				
Bias	−0.85	−2.66	−1.58	−1.28
Std	2.28	2.64	2.53	1.78
Corr	0.82	0.75	0.77	0.90
Rms	2.42	3.73	2.97	2.19
Slope	0.73	0.54	0.62	0.75
Int	4.93	7.41	6.78	4.29
NSA (133)				
Bias	−1.72	−2.43	−2.14	−1.69
Std	2.65	3.35	2.79	2.61
Corr	0.75	0.60	0.70	0.75
Rms	3.15	4.13	3.51	3.10
Slope	0.68	0.55	0.55	0.64
Int	3.76	5.34	5.60	4.51
TWP (51)				
Bias	2.40	17.14	6.41	1.13
Std	5.33	18.78	7.45	3.47
Corr	0.60	0.38	0.56	0.67
Rms	5.79	25.29	9.78	3.62
Slope	0.89	1.69	1.10	0.58
Int	6.98	−11.05	2.19	18.11
FKB (98)				
Bias	1.11	0.67	1.50	1.22
Std	3.53	4.95	4.10	3.18
Corr	0.78	0.77	0.78	0.82
Rms	3.68	4.97	4.35	3.40
Slope	0.84	1.17	1.00	0.88
Int	4.25	−2.70	1.48	3.62

[a]Using the Decker 0.95 model, Salonen model, Sal08 – Tuned, and CldMod, for the overall test data set and specific for ARM SGP Central Facilty in Oklahoma, PYE Mobile Facility in Point Reyes, California, NSA site in Barrow, Alaska, TWP site in Manus, Papua New Guinea, and FKB Mobile Facility in the Black Forest, Germany. Units are in kelvins.

with altitude considering clouds formed by adiabatic lifting, its value being a unique function of the height above the cloud base. In real clouds the LWC profile is disturbed by entrainment of dryer air, mixing, precipitation fallout, and radiative heating/cooling [*Korolev et al.*, 2007].

[37] The following model is proposed:

$$LWC = c \cdot z^a \cdot (1 - z^{a+1})^b \cdot p_w$$
$$IWC = c \cdot z^a \cdot (1 - z^{a+1})^b \cdot (1 - p_w) \quad (7)$$

where z is $\frac{h-h_b}{\Delta H}$ the altitude above the cloud base h_b (km) normalized with respect to the cloud thickness ΔH (km), h is the altitude above the station (in km), parameters a, b, c are given by

$$c(h, \Delta H) = \begin{cases} 0.8 \cdot RH(h) & \Delta H < 0.1\ km \\ 1.46 \cdot RH(h) \cdot \Delta H & 0.1 < \Delta H < 0.6\ km \\ 0.74 \cdot RH(h) & \Delta H > 0.6\ km \end{cases} \quad g \cdot m^3$$
$$a(z) = z/1.5$$
$$b(z) = 1.5 + z/1.5 \quad (8)$$

and p_W is given by

$$p_w(T) = \begin{cases} 1 & T \geq 0^\circ C \\ 1 - (T/35)^2 & -35 \leq T < 0^\circ C \\ 0 & T < -35^\circ C \end{cases} \quad (9)$$

The values of the parameters a, b, and c in equations (7)–(9) were obtained by tuning the simulated Tb values to the MWR measured Tb values at 31.4 GHz, letting the parameters vary according to the methodology described in section 5.1. About 5000 different combinations of the parameters were evaluated. We mention that the parameter c is not a continuous function of ΔH. This is due to the choice of having all the parameters (including the parameters that are part of c) vary independently on the grid.

[38] The proposed one is a simple function (derived from the distribution of *Kumaraswamy* [1980]) that is lower and upper bounded, chosen to resemble average LWC profiles as shown in the works of *Korolev et al.* [2007], and *van Meijgaard et al.* [2004], and parameterized by shape parameters a, b, and c. Several functions have been tested for the liquid water fraction function, including those used in the Decker and Salonen models, and the one proposed by *Pierdicca et al.* [2006]. Temperatures below which clouds were assumed to be glaciated were evaluated ranging from −20°C to −35°C.

[39] The scatterplot of the simulated Tb values applying the new model (hereafter referred to as CldMod) with the measured Tb values from the MWRs is shown in Figure 5. The comparison of the performances of the CldMod model with respect to the Sal08-Tuned model shows an improvement in term of RMS error of about 25%.

6. Validation at Arm Sites

[40] In this section, the new model CldMod, and the Sal08–Tuned described in section 5, were evaluated at the ARM sites, by using an independent data set with respect to that one used for the parameter training. Data were collected at SGP during the year 2005, the ARM PYE during March–September 2005 (even data set), the ARM NSA site during 2003–2004, the ARM TWP site during the 2005–2006 period, and finally at the ARM FKB during April–December 2007 (even data set). The Decker (0.95 threshold) and the Salonen model were also evaluated as a reference.

[41] In Table 4, we reported the statistical analysis in terms of bias, std, rms, corr, slope and intercept of Tb values from the MWR versus Tb values computed from the RAOBs at the 31.4–GHz channel for the Decker 0.95 model, the Salonen model, the Sal08–Tuned, and CldMod, for the overall data set and specific for the various sites. As can be noticed from Table 4, both the Decker 0.95 and CldMod provided good results in comparison with the radiometer measurements, with the CldMod reducing the RMS by about 16%. Improvements can be noticed in particular at SGP in Oklahoma (20%), and at TWP in the tropics (37%). With respect to the Salonen model, CldMod improved the RMS by more than 60%; the Sal08–Tuned provided an improvement of 47%, especially at TWP (60%), PYE (20%) and at NSA (15%).

[42] We point out the higher negative bias (−2.43 K), and a reduced slope (0.55) of the Salonen model with

Table 5. Comparison of Decker Density Profiles at ARM Sites[a]

ARM Site	Model–1	Model–2
All sites		
Bias	9.61	3.33
Std	13.90	6.89
Corr	0.69	0.83
Rms	16.89	7.65
Slope	1.55	1.23
Int	−2.63	−1.70
SGP		
Bias	15.28	5.82
Std	16.22	7.71
Corr	0.65	0.73
Rms	22.22	9.63
Slope	2.24	1.40
Int	−12.19	−3.02
PYE		
Bias	6.42	1.61
Std	7.05	3.47
Corr	0.70	0.77
Rms	9.50	3.81
Slope	1.62	1.04
Int	−7.10	0.80
NSA		
Bias	3.26	−0.02
Std	9.05	4.40
Corr	0.61	0.67
Rms	9.58	4.38
Slope	1.71	1.04
Int	−9.03	−0.68
TWP		
Bias	12.89	6.06
Std	18.18	9.75
Corr	0.51	0.55
Rms	22.13	11.39
Slope	2.28	1.40
Int	−39.64	−10.17
FKB		
Bias	13.10	5.25
Std	14.71	7.02
Corr	0.63	0.70
Rms	19.64	8.74
Slope	2.15	1.31
Int	−10.12	−0.93

[a]Model–1 refers to Decker density ranging from 0.2 to 0.8 g m^3, Model–2 to density ranging from 0.1 to 0.4 g m^3. Calculations minus MWR measurements (K) at 31.4 GHz.

respect to the other models at NSA in Alaska. Our analysis indicated that this difference is partly associated with the function chosen as fraction of cloud liquid (linear function), with a cloud glaciation temperature of -20°C. Conversely, using a function as in equation (9), coupled with assuming such temperature to be as low as -30 (Decker) or -35 (CldMod and Sal08–Tuned), improved the comparison with respect to the radiometer data. Nevertheless, some negative bias is still present in both the Decker model and the CldMod, suggesting that either a further investigation on the models (for example, by using site-specific coefficients) might be necessary, or the accuracy of microwave radiometers in such a cold and dry environment should be further investigated [*Racette et al.*, 2005; *Mattioli et al.*, 2007; *Cimini et al.*, 2007].

[43] A negative bias was also found in the comparison at PYE for all models, and more significant for the Salonen one (-2.66 K). Our analysis indicated that Tb values were generally referred to low stratiform clouds cases, with thickness less than 1 km. Few data collected at the tropics, where convection is the dominant atmospheric process, and measurements often reach saturation, were able to satisfy the selecting criteria used in our analysis (see sections 3.1 and 4). Nevertheless, such comparisons show features that are consistent with those inferred at SGP and at FKB. Specifically for the Salonen model, the high values of Tb that resulted in such a large RMS (25.3 K) were mainly produced because of the large cloud thicknesses provided by the model threshold (see section 3.1).

[44] As far as the analysis of the Decker cloud model is concerned, among the three cloud models given by *Decker et al.* [1978], and described in section 2.1, the third function, which has been utilized in this work (see Figure 3b and Table 5), is recommended. Comparisons performed at the ARM sites for the first two Decker cloud water contents (Model–1 and Model–2) are summarized in Table 5. Model–1 refers to content ranging from 0.2 to 0.8 g m^{-3} (corresponding to γ equal to 1), Model–2 to content ranging from 0.1 to 0.4 g m^{-3} (i.e., γ equal to 0.5). Both functions provided large RMS and biases (with the exception of Model-2 at NSA), at all the sites examined.

7. Conclusions

[45] The Decker and Salonen cloud models, currently in use in propagation and remote sensing simulations, were evaluated on the basis of the high quality controlled RAOBs and ceilometer measurements available at ARM SGP site, to verify their capability of cloud detection. The comparison evidenced that the Salonen RH threshold function provided poor results, mainly in the middle troposphere. To overcome this problem we modified the Salonen humidity threshold function by tuning it to the ceilometer data, obtaining an improvement of about 15% in the cloud detection and a reduction of about 26% in the false alarm rate with respect to the original Salonen threshold function.

[46] Decker, Salonen, and modified Salonen models were included in a radiative transfer algorithm to simulate brightness temperatures in cloudy conditions and in the absence of scattering. To evaluate the applicability of the various models to different environments, our analysis was performed by using data collected at several ARM sites, equipped with radiosonde release facility, ceilometer and dual-channel microwave radiometer. The comparison of Tb values measured by MWRs to simulated ones with Salonen models (even including a tuning of water content parameters) evidenced a poorer agreement with respect to what obtained comparing measurements to Decker 095 simulated Tb values. Then, a new formulation (CldMod) was proposed, considering also that the adiabatic formulation as in the Salonen model is generally not completely representative of low stratiform clouds.

[47] Both the Decker 0.95 model and CldMod are robust models for the cloud water content estimation at different geographical zones, with superior performances of CldMod able to reduce the overall RMS in the comparison with the MWRs at 31.4 GHz of about 16% with respect to Decker 0.95, and in particular at SGP in Oklahoma (20%), and in the tropics (37%). Moreover, we have developed and validated in almost all climatic zones a new model for describing a cloud in terms of its boundaries and water distribution.

[48] **Acknowledgments.** Data were obtained from the Atmospheric Radiation Measurement (ARM) Program sponsored by the U.S. Department of Energy, Office of Science, Office of Biological and Environmental Research, Environmental Sciences Division.

References

Al-Ansari, K., P. Garcia, J. M. Riera, and A. Benarroch (2003), One-year cloud attenuation results at 50 GHz, *Electron. Lett.*, *39*(1), 136–137.

Alouini, M. S., S. A. Borgsmiller, and P. G. Steffes (1997), Channel characterization and modeling for Ka-band very small aperture terminals, *Proc. IEEE*, *85*(6), 981–997.

Altshuler, E., and R. Marr (1989), Cloud attenuation at millimeter wavelengths, *IEEE Trans. Antennas Propag.*, *37*(11), 1473–1479.

Basili, P., S. Bonafoni, V. Mattioli, P. Ciotti, and E. R. Westwater (2006), Cloud model studies for the simulation of brightness temperatures, paper presented at the International Geoscience and Remote Sensing Symposium, Inst. of Electr. and Electron. Eng., Denver, Colo., 31 July to 4 Aug.

Bouchard, P. (2005), Improved algorithm for detecting cloud layers and amounts using retrievals from a surface-based

multifrequency profiling radiometer, in *Remote Sensing of Clouds and the Atmosphere X*, edited by K. Schafer et al., Proc. SPIE, vol. 5979, 597903.

Bouchard, P., and D. V. Rogers (2006), Statistics on low-lying liquid and liquid-dominant mixed-phase clouds over Ottawa, paper presented at the European Conference on Antennas and Propagation (EuCAP), Eur. Space Agency, Nice, France, 6 – 10 Nov.

Boudala, F. S., G. A. Isaac, S. G. Cober, and Q. Fu (2004), Liquid fraction in stratiform mixed-phase clouds from in situ observations, *Q. J. R. Meteorol. Soc.*, *130*, 2919 – 2931.

Castanet, L., J. Lemorton, T. Konefal, A. K. Shukla, P. A. Watson, and C. L. Wrench (2001), Comparison of various methods for combining propagation effects and predicting loss in low-availability systems in the 20 – 50 GHz frequency range, *Int. J. Satell. Commun.*, *19*, 317 – 334.

Chernykh, I. V., and R. E. Eskridge (1996), Determination of cloud amount and level from radiosonde soundings, *J. Appl. Meteorol.*, *35*(8), 1362 – 1369.

Cimini, D., E. R. Westwater, A. J. Gasiewski, M. Klein, V. Leuski, and J. C. Liljegren (2007), Ground-based millimeter- and submillimiter-wave observations of low vapor and liquid water contents, *IEEE Trans. Geosci. Remote Sens.*, *45*(7), 2169 – 2180.

Decker, M. T., E. R. Westwater, and F. O. Guiraud (1978), Experimental evaluation of ground-based microwave radiometric sensing of atmospheric temperature and water profiles, *J. Appl. Meteorol.*, *17*, 1788 – 1795.

Dintelmann, F., and G. Ortgies (1989), Semiempirical model for cloud attenuation prediction, *Electron. Lett.*, *25*(22), 1487 – 1488.

Dissanyake, A., J. Allnut, and F. Haidara (1997), A prediction model that combines rain attenuation and other propagation impairments along earth satellite paths, *IEEE Trans. Antennas Propag.*, *45*, 1546 – 1558.

Dissanayake, A., J. Allnutt, and F. Haidara (2001), Cloud attenuation modeling for SHF and EHF applications, *Int. J. Satell. Commun.*, *19*, 335 – 345.

Garcia, P., A. Benarroch, and J. M. Riera (2008), Spatial distribution of cloud cover, *Int. J. Satell. Commun. Network.*, *26*, 141 – 155.

Green, H. E. (2004), Propagation impairment on Ka-band SATCOM links in tropical and equatorial regions, *IEEE Antennas Propag. Mag.*, *46*(2), 31 – 46.

Gultepe, I., G. A. Isaac, and S. G. Cober (2002), Cloud microphysical characteristics versus temperature for three Canadian field projects, *Ann. Geophys.*, *20*, 1891 – 1898.

Han, Y., and E. Westwater (1995), Remote sensing of tropospheric water vapor and cloud liquid water by integrated ground-based sensors, *J. Atmos. Oceanic Technol.*, *12*, 1050 – 1059.

Hanssen, R. (1998), Atmospheric heterogeneities in ERS Tandem SAR interferometry, *DEOS Rep. 98.1*, 136 pp., Delft Univ. Press, Delft, Netherlands.

ITU-R (1999), Attenuation due to clouds and fog, *ITU-R Recomm. P.840-3*, Geneva, Switzerland.

ITU-R (2007), Attenuation by atmospheric gases, *ITU-R Recomm. P.676-7*, Geneva, Switzerland.

Korolev, A. V., G. A. Isaac, S. Cober, J. W. Strapp, and J. Hallett (2003), Microphysical characterization of mixed-phase clouds, *Q. J. R. Meteorol. Soc.*, *129*, 39 – 66.

Korolev, A. V., G. A. Isaac, J. W. Strapp, S. G. Cober, and H. W. Barker (2007), In situ measurements of liquid water content profiles in midlatitude stratiform clouds, *Q. J. R. Meteorol. Soc.*, *133*, 1693 – 1699.

Kumaraswamy, P. (1980), A generalized probability density function for double-bounded random processes, *J. Hydrol. Amsterdam*, *46*, 79 – 88.

Lemorton, J., L. Castanet, V. Hout, and T. Marsault (2001), A new opportunity for EHF propagation experiments: The EXPRESS campaign with the satellite STENTOR, *Int. J. Satell. Commun.*, *19*, 347 – 362.

Lemus, L., L. Rikus, C. Martin, and R. Platt (1997), Global cloud liquid water path simulations, *J. Clim.*, *10*, 52 – 64.

Liebe, H. J. (1989), MPM, An atmospheric millimeter wave propagation model, *Int. J. Infrared Millimeter Waves*, *10*(6), 631 – 650.

Liebe, H. J., G. A. Hufford, and T. Manabe (1991), A model for the complex permittivity of water at frequencies below 1 THz, *Int. J. Infrared Millimeter Waves*, *12*(7), 659 – 675.

Liljegren, J. C. (2000), Automatic self-calibration of ARM microwave radiometers, in *Microwave Radiometry and Remote Sensing of the Earth's Surface and Atmosphere*, edited by P. Pampaloni and S. Paloscia, pp. 433 – 443, VSP, Utrecht, Netherlands.

Luini, L., C. Riva, C. Capsoni, and A. Martellucci (2007), Attenuation in non rainy conditions at millimeter wavelengths: Assessment of a procedure, *IEEE Trans. Geosci. Remote Sens.*, *45*(7), 2150 – 2157.

Mandeep, J. S., and S. I. S. Hassan (2008), Cloud attenuation in millimeter wave and microwave frequencies for satellite applications over equatorial climate, *Int. J. Infrared Millimeter Waves*, *29*, 201 – 206.

Martellucci, A., et al. (2002a), Radiowave propagation modelling for SatCom services at Ku-band and above, in *COST Action 255 Final Report*, edited by R. A. Harris, Eur. Space Agency Spec. Publ., *ESA SP-1252*.

Martellucci, A., J. P. V. Poiares Baptista, and G. Blarzino (2002b), New climatological databases for ice depolarisation on satellite radio links, paper presented at COST Action 280 1st International Workshop, QinetiQ, Malvern, U. K, July.

Mattioli, V., E. R. Westwater, S. I. Gutman, and V. R. Morris (2005), Forward model studies of water vapor using scanning microwave radiometers, Global Positioning System, and radiosondes during the Cloudiness Inter-Comparison Experiment, *IEEE Trans. Geosci. Remote Sens.*, *43*(5), 1012 – 1021.

Mattioli, V., P. Basili, S. Bonafoni, P. Ciotti, L. Pulvirenti, N. Pierdicca, F. S. Marzano, F. Consalvi, E. Fionda, and E. R. Westwater (2006), Cloud liquid models for propagation studies: Evaluation and refinements, paper presented at the

European Conference on Antennas and Propagation (EuCAP), Eur. Space Agency, Nice, France, 6 –10 Nov.

Mattioli, V., E. R. Westwater, D. Cimini, J. S. Liljegren, B. M. Lesht, S. I. Gutman, and F. J. Schmidlin (2007), Analysis of radiosonde and ground-based remotely sensed PWV data from the 2004 North Slope of Alaska Arctic Winter Radiometric Experiment, *J. Atmos. Oceanic Technol.*, *24*(3), 415–431.

Miloshevich, L. M., H. Vömel, D. N. Whiteman, B. M. Lesht, F. J. Schmidlin, and F. Russo (2006), Absolute accuracy of water vapor measurements from six operational radiosonde types launched during AWEX-G and implications for AIRS validation, *J. Geophys. Res.*, *111*, D09S10, doi:10.1029/2005JD006083.

Minnis, P., Y. Yi, J. Huang, and K. Ayers (2005), Relationships between radiosonde and RUC-2 meteorological conditions and cloud occurrence determined from ARM data, *J. Geophys. Res.*, *110*, D23204, doi:10.1029/2005JD006005.

Naud, C. M., J.-P. Muller, and E. E. Clothiaux (2003), Comparison between active sensor and radiosonde cloud boundaries over the ARM Southern Great Plains site, *J. Geophys. Res.*, *108*(D4), 4140, doi:10.1029/2002JD002887.

Pierdicca, N., L. Pulvirenti, and F. S. Marzano (2006), A model to predict cloud density from mid-latitude atmospheric soundings for microwave radiative transfer applications, *Radio Sci.*, *41*, RS6005, doi:10.1029/2006RS003463.

Racette, E. P., et al. (2005), Measurement of low amounts of precipitable water vapor using ground-based millimeterwave radiometry, *J. Atmos. Oceanic Technol.*, *22*(4), 317–337.

Rosenkranz, P. W. (1998), Water vapor microwave continuum absorption: A comparison of measurements and models, *Radio Sci.*, *33*(4), 919–928.

Rosenkranz, P. W. (1999), Correction to water vapor microwave continuum absorption: A comparison of measurements and models, *Radio Sci.*, *34*(4), 1025.

Salonen, E., and W. Uppala (1991), New prediction method of cloud attenuation, *Electron. Lett.*, *27*(12), 1106–1108.

Sarkar, S. K., I. Ahmad, J. Das, and A. K. De (2005), Cloud height, cloud temperature and cloud attenuation in microwave and millimeter wave frequency bands over Indian tropical east cost, *Int. J. Infrared Millimeter Waves*, *26*, 329–340.

Schmidlin, F. J., J. K. Luers, and P. D. Huffman (1986), Preliminary estimates of radiosonde thermistor errors, *NASA Tech. Rep., NAS 1.602637*, 15 pp.

Schroeder, J. A., and E. R. Westwater (1991), Users' guide to WPL microwave radiative transfer software, *NOAA Tech. Rep. ERL-219 WPL-213*, 84 pp., NOAA Environ. Res. Lab., Boulder, Colo.

Slobin, S. D. (1982), Microwave noise temperature and attenuation of clouds: Statistics of these effects at various sites in the United States, Alaska and Hawaii, *Radio Sci.*, *17*, 1443–1454.

Turner, D. D., B. M. Lesht, S. A. Clough, J. C. Liljegren, H. E. Revercomb, and D. C. Tobin (2003), Dry bias and variability RS80-H radiosondes: The ARM experience, *J. Atmos. Oceanic Technol.*, *20*, 117–132.

Ulaby, F. T., R. K. Moore, and A. K. Fung (Eds.) (1981), Microwave Remote Sensing: Active and Passive, vol. 1, *Microwave Remote Sensing Fundamentals and Radiometry*, 456 pp., Addison-Wesley, Reading, Mass.

van Meijgaard, E., S. Crewell, and U. Löhnert (2004), Analysis of model predicted liquid water path and liquid water vertical distribution using observations from CLIWA-NET, paper presented at the 4th Study Conference on BALTEX, Gudhjem, Bornholm, Denmark, May .

Vömel, H., H. Selkirk, L. Miloshevich, J. Valverde, J. Valdés, E. Kyrö, R. Kivi, W. Stolz, G. Peng, and J. A. Diaz (2007), Radiation dry bias of the Vaisala RS92 humidity sensor, *J. Atmos. Oceanic Technol.*, *24*, 953–963.

Wang, D., J. Carlson, D. B. Parsons, T. F. Hock, D. Lauritsen, H. L. Cole, K. Beierle, and E. Chamberlain (2003), Performance of operational radiosonde humidity sensors in direct comparison with a chilled mirror dew-point hygrometer and its climate implication, *Geophys. Res. Lett.*, *30*(16), 1860, doi:10.1029/2003GL016985.

Wang, J., W. B. Rossow, and Y.-C. Zhang (2000), Cloud vertical structure and its variations from a 20-year global rawinsonde data set, *J. Clim.*, *13*, 3041–3056.

Wang, J., H. Cole, D. J. Carlson, E. R. Miller, K. Beierle, A. Paukkunnen, and T. K. Laine (2002), Corrections of humidity measurement errors from the Vaisala RS80 radiosonde—Applications to TOGA COARE data, *J. Atmos. Oceanic Technol.*, *19*, 981–1002.

Watson, P. A., and Y. F. Hu (1994), Prediction of attenuation on satellite-earth links for systems operating with low fade margins, *Proc. Inst. Elect. Eng., Microw. Antennas Propag.*, *141*, 467–472.

Westwater, E. R. (1972), Microwave emissions from clouds, *Tech. Rep. ERL-219 WPL 18*, 43 pp., NOAA Environ. Res. Lab., Boulder, Colo.

Westwater, E. R. (1993), Ground-based microwave remote sensing of meteorological variables, in *Atmospheric Remote Sensing by Microwave Radiometry*, edited by M. A. Janssen, pp. 145–213, John Wiley, New York.

Wrench, C. L., P. G. Davies, and J. Ramsden (1999), Global prediction of slant path attenuation on Earth space links at EHF, *Int. J. Satell. Commun.*, *17*, 177–186.

P. Basili, S. Bonafoni, and V. Mattioli, Dipartimento di Ingegneria Elettronica e dell'Informazione, Università di Perugia, via G. Duranti 93, I-06125 Perugia, Italy. (vinia.mattioli@diei.unipg.it)

P. Ciotti, Dipartimento di Ingegneria Elettrica e dell'Informazione, Università di L'Aquila, I-67040 Poggio di Roio, L'Aquila, Italy. (cpiero@ing.univaq.it)

E. R. Westwater, Center for Environmental Technology, Department of Electrical and Computer Engineering, University of Colorado, Boulder, CO 80309, USA. (ed.westwater@colorado.edu)